JOURNAL OF GEOPHYSICAL RESEARCH: ATMOSPHERES, VOL. 118, 8448–8459, doi:10.1002/jgrd.50656, 2013

Space-time variability of the rainfall over the western Mediterranean region: A statistical analysis

J.-F. Rysman,[1] S. Verrier,[2,3] Y. Lemaître,[2] and E. Moreau[4]

Received 3 December 2012; revised 28 June 2013; accepted 16 July 2013; published 15 August 2013.

[1] This study aims at better understanding the space-time statistical properties of rain over a Mediterranean region. To this end we analyzed temporal, spatial, and spatio-temporal spectra of rain field maps provided by an X-band radar situated in the southeast part of France. The database extends from 2009 to 2012 and has a spatial and temporal resolution of 1 km^2 and 5 min. The analysis highlights several scaling regimes, which are interpreted in terms of meteorological structures (convective cells, mesoscale structures, and midlatitude cyclones). The analysis of spectra per month confirms the dependency of the spectral signature to the underlying meteorological process. Nevertheless, our results also reveal that for a given range of scales (20–45 min in time and 7–20 km in space), spectral slope is monthly invariant. It means that rain behaves identically, in terms of scaling, whatever the mechanism that generated it (convection, front). Moreover, spectral analysis shows that the temporal decorrelation scale is 10 days, which can possibly be related to the longest lifetime of a meteorological phenomenon in the region (i.e., about 10 days). An approach to compute the scaling anisotropy between space and time is proposed. It reveals that, over two distinct ranges of scales (7–20 km/20–45 min and 20–70 km/45 min–3 h), the scaling anisotropic coefficient is equal to 2. It also reveals that the ratio of spectral slope of 2-D angle averaged spatial spectrum versus 1-D temporal spectrum is equal to 1 over these ranges of scales. It suggests a similarity in the second-order properties (e.g., correlation) of temporal and spatial rain field. All these results are important to better understand rainfall statistical behavior and could also be used for the development of downscaling schemes and the validation of numerical weather models.

Citation: Rysman, J.-F., S. Verrier, Y. Lemaître, and E. Moreau (2013), Space-time variability of the rainfall over the western Mediterranean region: A statistical analysis, *J. Geophys. Res. Atmos.*, *118*, 8448–8459, doi:10.1002/jgrd.50656.

1. Introduction

[2] Rainfall processes in the western part of the Mediterranean region are characterized by an important spatial and temporal variability. Because of its latitude (between 36°N and 44°N), the region is affected both by the midlatitude low-pressure belt and by the subtropical highs. In particular, during winter, the region is constantly affected by frontal precipitations generated by midlatitude disturbances. During the summer, the weather is drier because of the Azores anticyclone. Nevertheless, deep convection frequently occurs during the afternoon [*Funatsu et al.*, 2009]. Other factors such as North Atlantic Oscillation, convergence zones, and mountains influence the precipitation of this region [see *Boudevillain et al.*, 2009]. The western Mediterranean region has also one of the world's highest density of cyclogenesis [*Pettersen*, 1956; *Hoskins and Hodges*, 2002; *Wernli and Schwierz*, 2006].

[3] All these processes influence the rainfall and can cause dryness or severe floods over this region. For instance, the Draguignan region in the south of France was affected by a recent flood (15–16 June 2010) that caused 20 casualties and damages estimated at more than 500 million euros [*Moreau and Roumagnac*, 2010]. Since more than 150 millions people live in the Mediterranean region, study and prevention of such disasters are crucial. For this purpose, an X-band polarimetric and Doppler radar called Hydrix has been installed close to Nice (southeastern France) in 2007 in the frame of FRAMEA project (Flood forecasting using Radars in Alpine and Mediterranean Areas) [*Testud et al.*, 2007]. This radar measures rain with spatial and temporal resolutions of respectively, 1 km^2 and 5 min. The established database extends from 2009 to 2012. The high resolution and

[1]UPMC Univ. Paris 06, Université Versailles St-Quentin, CNRS/INSU, LATMOS-IPSL, Guyancourt, France.
[2]Université Versailles St-Quentin, CNRS/INSU, LATMOS-IPSL, Guyancourt, France.
[3]Now at LOCEAN-IPSL, CNES, Paris, France.
[4]Novimet, Guyancourt, France.

Corresponding author: J.-F. Rysman, LATMOS, 11 Boulevard d'Alembert, 78280 Guyancourt, France. (jean-francois.rysman@latmos.ipsl.fr)

2169-897X/13/10.1002/jgrd.50656

wide temporal extension of measurements associated to the diversity of rainfall processes found in this region make this data set particularly valuable and gives the possibility to analyze statistically the space-time variability of precipitation under various meteorological conditions.

[4] Every meteorological process from the synoptic scale to the scale of droplets formation impacts the temporal and spatial characteristics of rain. Thus, precipitation involve a large spectrum of phenomena whose respective contributions are extremely difficult to diagnose and for some of them to forecast. However, numerous authors [*Fraedrich and Larnder*, 1993; *Olsson et al.*, 1993; *Tessier et al.*, 1993; *Fabry*, 1996; *Over and Gupta*, 1996; *Deidda*, 1999; *Nykanen and Harris*, 2003; *Lovejoy and Schertzer*, 2008; *Mandapaka et al.*, 2009; *Verrier et al.*, 2011] showed that despite this complexity, rainfall variability is characterized by an empirical scale-invariance. Scale-invariance (or self-similarity) implies that the statistical moments of rainfall follow a power law whose exponent remains constant over a range of scales. Moreover, several studies [*Over and Gupta*, 1994, 1996; *Perica and Foufoula-Georgiou*, 1996; *Harris et al.*, 1996; *Purdy et al.*, 2001; *Nykanen and Harris*, 2003; *Nykanen*, 2008] showed that various scaling exponents are influenced by the implied meteorological processes (synoptic weather, CAPE, orography).

[5] In this context, this paper aims at investigating statistically the spatial and temporal variability of rain in terms of meteorological processes over the western Mediterranean region. Understanding of the space-time variability of rainfall over various ranges of scales is particularly valuable for meteorologists and hydrologists either to analyze the involved processes or to develop downscaling methods for local rain estimate from space-borne observations or large-scale numerical models [see *Olsson*, 1998; *Biaou*, 2004; *Rebora et al.*, 2006].

[6] The paper is organized as follows. Section 2 presents the data set used in this study. Section 3 introduces the analysis tools. Section 4 highlights the main characteristics of the precipitation observed by the radar. First, we present and interpret in terms of meteorological processes the one-dimensional temporal and spatial spectra of rainfall. Then we analyze the spatio-temporal field by computing two-dimensional space-time spectra and scaling anisotropy coefficient. The discussion and conclusion are given in section 6.

2. Data

[7] The rainfall dataset is derived from radar measurements performed by an X-band polarimetric and Doppler radar, called Hydrix, located at Mont Vial (1500 m) close to Nice in the southeastern France (Figurel). Technical information about this radar can be found in *Le Bouar et al.* [2008] and *Moreau et al.* [2009]. In order to convert the radar reflectivity (i.e., the reflected electromagnetic signal) into rainfall intensity, the ZPHI algorithm [*Testud et al.*, 2000] is applied. This algorithm corrects from beam attenuation along each radial and then computes the N_0^* parameter derived from the drop size distribution $N(d)$ in order to retrieve the rain rate through the relation (equation (1)):

$$R = a(N_0^*)^{1-b} Z^b \tag{1}$$

where R is the rain rate (mm/h), a and b are two constant empirical coefficients, and Z is the reflectivity (dBz). An estimation of rain at ground is performed using a weight average of the rainfall obtained at multiple elevations. Weights take into account the altitude of measurements, the precipitation phase, and the beam masking. For a more detailed description of this method. see *Le Bouar et al.* [2008]. Rainfall data validation has been performed by comparison with S-band radar observations [*Diss et al.*, 2009] and rain gage measurements [*Moreau et al.*, 2009].

[8] The rainfall database extends continuously from March 2009 until today. The spatial resolution is 1 × 1 km and the temporal resolution is 5 min. Most of interruptions last only a few hours (the longest six interruptions lasted between 3 and 7 days). In order to get a regular sampling, linear interpolation was performed for interruptions shorter than 1 h and rain was set to zero for interruptions longer than 1 h. This method does not impact significantly the statistical properties because missing data represent less than 5% of the full time series. Another issue comes from the radar signal attenuation with distance. Indeed, in spite of the correction of radar attenuation along each radial beam, the rainfall measurement can be affected by remaining attenuation in case of strong rain. As a result, in order to minimize errors on the highlighted rainfall statistical properties, radar measurements are restricted to a 100 km radius.

3. Scaling Behavior

[9] As discussed above, numerous authors demonstrated the presence of scale invariance in various meteorological fields. This section describes the spectral analysis, which permits to highlight the scaling behavior of rain and shows how to link scaling properties and meteorological processes.

3.1. Spectral Analysis

[10] Spectral analysis, just like other tools such as autocorrelation and variograms [see *Creutin and Obled*, 1982; *Lebel et al.*, 1987; *Berne et al.*, 2004; *Barros et al.*, 2004; *Berne et al.*, 2009; *Kirstetter et al.*, 2010; *Molinié et al.*, 2012; *Mandapaka et al.*, 2012], allows to investigate the second-order properties of a field. It has been shown that if a physical process presents a scale-invariance in the time or space domain, its power spectral density exhibits a power law behavior in the frequency domain (equation (2)):

$$P(f) \sim f^{-\beta} \sim T^{\beta} \tag{2}$$

where f is the frequency and T the period.

[11] Decrease of $P(f)$ with frequency is related to the increase of the mean variance with period. The β value shows how fast this increase is. In other words, it shows how fast the autocorrelation (the autocorrelation is the Fourier transform of the power spectral density) decreases with lag. The faster the autocorrelation decreases, the lower the β value is. In the limit, a white noise has a β exponent equal to zero whereas a highly correlated process has a high β value. A way to understand this concept is to consider a Brownian motion. For example, a Brownian motion is highly correlated at a given time $t + 1$ with time t and is less and less

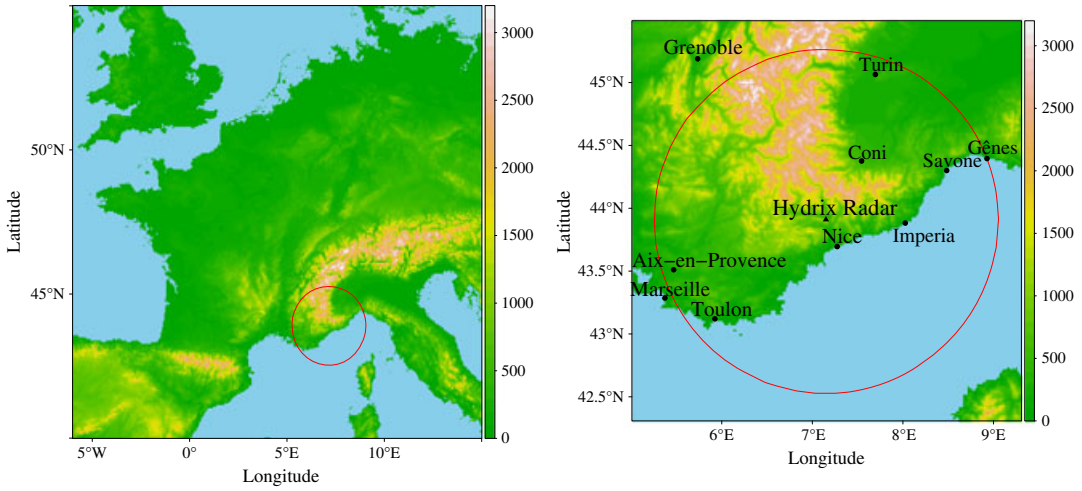

Figure 1. Area covered by the radar Hydrix.

correlated as far as the lag increases. As a result, mean variance at $lag(1)$ is lower than mean variance at $lag(n > 1)$. Moreover, if diffusivity coefficient associated to a Brownian motion is very important, then the autocorrelation decreases strongly with lag and the spectral slope is low.

[12] The power law behavior of power spectral density has been widely used to highlight the scaling behavior of various geophysical fields such as morphology of fractured rock surfaces [*Schmitt and Scholz*, 1995], wind and temperature [*Gage and Nastrom*, 1986] or radar reflectivity [*Tessier et al.*, 1993]. Concerning rainfall, temporal [*Fraedrich and Larnder*, 1993] and spatial [*Mandapaka et al.*, 2009] spectral analysis revealed a scaling behavior over a wide range of scales.

[13] No theory fully explains the observed scaling behavior of rain, but because rain is strongly coupled with wind, the rainfall scaling behavior could be related to the theory of turbulent fields [see *Kolmogorov*, 1941; *Obukhov*, 1949; *Corrsin*, 1951; *Kolmogorov*, 1962]. In the framework of this theory, Kolmogorov showed in 1941, that the spectrum of velocity increments within an isotropic turbulent flow has a β exponent equal to 5/3. Later, Corrsin and Obukhov showed that the spectrum of the concentration of a passive scalar is also scaling with the same 5/3 exponent. For a more detailed discussion about rain and turbulence, see *Lovejoy and Schertzer* [2008].

[14] Space and time are not independent for rainfall processes. For example, a rain cell advected by winds induces a space and time relationship. It is why we conducted a space-time spectral analysis. Indeed, 2-D analysis highlights the relations between space and time in the frequency domain through their respective scaling behavior and gives information about the space-time characteristics of a given meteorological situation in the real space.

[15] In the present study, the β spectral exponent is computed by performing a linear regression of the logarithm of the frequency versus the logarithm of the power spectral density over a range of scales (temporal or spatial).

[16] In this section, we explained that the value of the exponent of the power law depends on the mean variance between scales. In the next section, we explain that it is possible to link this exponent and the scaling regimes to meteorological processes.

3.2. Scaling Properties and Meteorological Processes

[17] The main objective of this section is to relate empirical scaling behavior of rainfall to meteorological processes.

[18] First, we have to overcome some difficulties related to rainfall behavior. Indeed, the rainfall is very often intermittent. It means that the measured signal is the superposition of the rain signal and the so-called support (meaning the combination of rain and no rain). These two components of the spectrum cannot be easily separated. The only way to get the intrinsic statistical properties of the rain is to extract and to analyze the rainfall signal only for periods of continuous rain. If we do not, the support impacts the spectra as shown by *de Montera et al.* [2009] and *Verrier et al.* [2011]. In particular, these authors showed that dry periods in time series of rain tend to decrease spectral slope. These dry periods are governed by physical processes. For instance, gravity waves can produce periodic patterns of rain/no rain areas. Obviously, this has a signature on the support. Thus, the support itself is related to the underlying physical processes. In this study we kept the full time series including the zero rain data, i.e., both rain and support signature.

[19] The instrumental approach to measure rainfall is also important: for example, radar measurements have a decreasing spatial resolution with distance because of the increasing

Table 1. Spatial and Temporal Typical Scales Depending on Rossby Number

Meteorological Scale	Rossby Number	Spatial Scale	Temporal Scale
Front	$\sim 10^{-1}$	1000 km	30 h
Mesoscale convective system	~ 1	100 km	3 h
Storm	~ 10	10 km	15 min

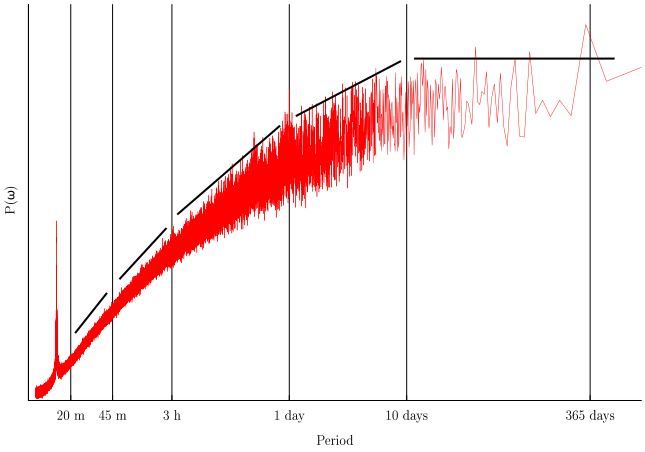

Figure 2. Energy spectral density versus temporal period in a log-log plot.

beam width. It means that the analysis of small scales must be handled with care and that a critical eye on results is important before any conclusion. Concerning radar, another problem appears when the freezing level is at low altitude because radar does not measure rain anymore but snow. Therefore, the question is as follows: Are snow and rain equivalent in terms of scaling properties? *Fabry* [1996] showed that snow and rain have a different scaling behavior but for very small scales (∼100 m and ∼10 sec) compared to the resolutions considered in this study.

[20] Eventually, various other processes can impact rainfall scaling behavior such as instrumental artifact or noise, which must be taken into account.

[21] *Purdy et al.* [2001], *Nykanen and Harris* [2003], and *Nykanen* [2008] showed experimentally that the β spectral exponent depends of the meteorological processes. They showed in particular that rain events associated to convective processes have higher β exponents than those associated to stratiform processes. Thus, it means that the scaling regimes of rainfall spectra could be explained by the underlying dynamical processes that generate rain and that we need to know the typical scales of these processes. A possibility is to observe the typical scales of meteorological processes that occur over the studied region as did *Fraedrich and Larnder* [1993], *Olsson et al.* [1993], and *Fabry* [1996].

[22] It is also possible to estimate the typical scales of these processes through a scale analysis of the equations of motion. The horizontal motions are governed by the horizontal momentum equations. If the viscosity terms are neglected, the horizontal projection on the x axis is

$$\frac{\mathrm{d}u}{\mathrm{d}t} = fv - \frac{1}{\rho}\frac{\partial P}{\partial x}$$

where u, v is the horizontal velocity, P the pressure, ρ the atmospheric density, and f the Coriolis factor.

[23] The Rossby number allowing this scale analysis is defined by the ratio between the acceleration and the Coriolis force:

$$Ro = \frac{\mathrm{d}u/\mathrm{d}t}{fv} \sim \frac{U}{f_o L}$$

where U is the characteristic horizontal velocity and L is the characteristic horizontal dimension (for details, see *Holton* [1992]). It characterizes the influence on motion of the Earth's rotation with respect to other processes. At the Mediterranean latitude, typical values for wind velocity and Coriolis factor are $U \sim 10$ m/s and $f_o \sim 10^{-4}\ s^{-1}$. Therefore, typical temporal and spatial scales of meteorological processes with respect to Rossby value can be estimated (see *Orlanski* [1975], *Atkinson* [1981] and Table 1). A high value of the Rossby number (order of magnitude ∼10) corresponds to storm scale (or convective scale). It is the size of isolated thunderstorms with typical temporal and spatial scales of about 15 min and 10 km, respectively. A low value of the Rossby number (OoM ∼0.1) corresponds to synoptic scales (midlatitude cyclones) with typical temporal and spatial scales of 30 h and 1000 km. Intermediate values of the Rossby number (OoM ∼1) correspond to the mesoscale (convective clusters) with typical temporal and spatial scales of 3 h and 100 km. Since for these different scales the primary forces (Coriolis, pressure, gravity,...) and thus the associated dynamical processes are not the same, we might expect the corresponding rainy structures to show different statistical properties. If we now make the hypothesis that a constant slope (i.e., a scaling regime) is associated to a dynamical process, breaks are expected in the spectra, each break giving roughly the typical scale of the rainfall process. Therefore, we can link the different scale ranges in space and in time of the spectra with meteorological processes.

4. One Dimensional Spectral Analysis

[24] As explained in the introduction, the first part of this work is devoted to one-dimensional analyses for time and space separately. The power spectral density of rainfall is computed and compared to previous works. Then the identify scaling regimes are interpreted in terms of meteorological processes.

4.1. Temporal Analysis

[25] The temporal power spectral density is obtained as follows: each radar map (resolution 1 × 1 km) is uniformly averaged on a grid with a resolution of 5 km^2. Then, for each grid box, the temporal Fourier transform (5 min resolution) is computed. Finally the mean of all the temporal spectra obtained is computed.

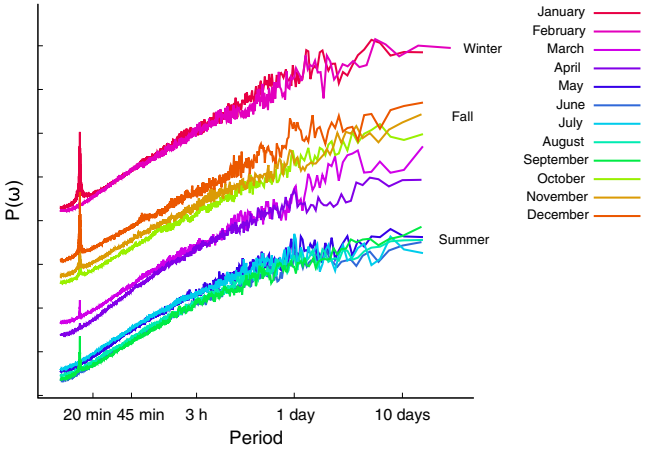

Figure 3. Energy spectral density versus temporal period in a log-log plot by month.

Table 2. Temporal Spectral Slopes for Winter, Summer, and Fall Per Scaling Range

Season	20–45 min	45 min–3 h	3 h–1 day	1–10 days
Winter	1.49 ± 0.05	1.35 ± 0.09	1.19 ± 0.23	0.67 ± 0.3
Summer	1.49 ± 0.05	1.01 ± 0.02	0.7 ± 0.07	0.12 ± 0.06
Fall	1.11 ± 0.13	1.06 ± 0.11	0.97 ± 0.18	0.67 ± 0.3

[26] The aggregation results in increasing correlation (organization) within the field as shown by *Olsson et al.* [1999], and as a result, it increases the slope of the computed spectrum. Nevertheless, in the present case, the impact of this aggregation is certainly weak. Indeed, *Olsson et al.* [1999] found that the increase of spectral slope was about 30% for an aggregation of the rainfall field over 500 km^2 area.

[27] The resulting temporal spectrum is shown in Figure 2. The reader must note that the abscissa corresponds to the time period. The spectrum is scaling down to 10 days and shows five different domains of scale invariance. Between 20 and 45 min, the spectrum presents a power law with an exponent of about 1.31, between 45 min and 3 h of about 1.02, between 3 h and 1 day of about 0.79 and between 1 and 10 days of about 0.46. For periods greater than 10 days, the spectrum presents a spectral plateau (exponent 0.09). It means that, for periods larger than 10 days, mean variance between 2 points does not increase anymore, i.e., correlation between rain events does not exist anymore. Comparison with past studies shows that these exponents agree with those previously found [e.g., *Fraedrich and Larnder*, 1993; *Olsson*, 1995; *Fabry*, 1996; *Verrier et al.*, 2011]. The different regimes (domains of scale invariance) also match well with those previously found except that the 20–45 min regime is not always highlighted in these studies.

[28] For scales lower than 15 min, we can notice the flattening of the spectrum. This behavior is probably due to instrumental accuracy and has already been noticed by *Fabry* [1996] and *de Montera et al.* [2009].

[29] The 15 min peak is related to the scanning strategy of the radar. Indeed, the radar scanning cycle is composed of three subcycles of 5 min in order to produce 5 min rainfall estimation. During test phases, the third part of the cycle is used with various operational modes, which slightly modifies the rain rate estimation. Concretely, this effect corresponds to the multiplication of the signal by a value slightly higher than 1 per 15 min. It does not impact the scaling properties of rainfall at other frequencies.

[30] Meteorological processes associated to rainfall in the Mediterranean region vary during the year. In order to see their effects on rainfall spectra, we computed temporal spectra per month. Figure 3 shows that the spectra can be split roughly in three classes: winter months (January to March), summer months (June to August) and fall months (October to December). Spring months show a mix signal between winter and summer months. Between 20 and 45 min every spectrum has roughly the same scaling regime with a slope of about 1.49 ± 0.05 except for fall months, which have a lower slope (1.11 ± 0.13). For summer months, a break occurs at 45 min and a second scaling regime extends between 45 min and 3 h (slope ∼1.01 ± 0.02). For other months, no break occurs but the slopes are slightly lower than for 20–45 min period (1.35 ± 0.09 for winter and 1.06 ± 0.11 for the fall). Two other breaks are found for every spectra at 3 h and 1 day (corresponding slope for summer: 0.7 ± 0.07, winter: 1.19 ± 0.23 and fall: 0.97± 0.18). Greater than 1 day, the spectra remains scaling up to 10 days during winter and fall months (0.67 ± 0.3) whereas in summer the slope is close to zero (0.12 ± 0.06). Higher than 10 days, every spectra show the spectral plateau. These results are summarized in Table 2.

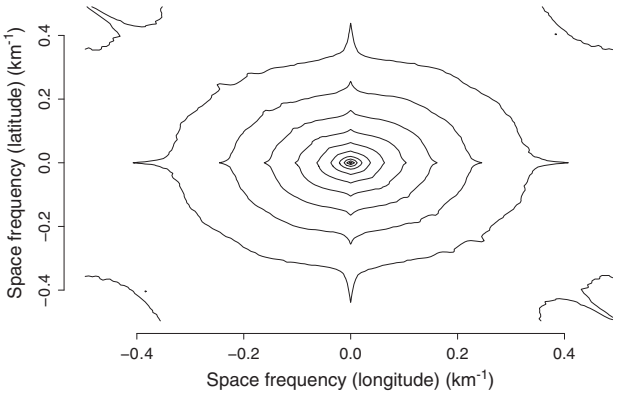

Figure 4. Level map of the logarithm of the power spectral density (x-y) computed between June 2009 and December 2011.

[31] The previous discussion on dynamical scale (section 3.2), indicates that the accessible scales in the present analysis cover convective scale (partially), mesoscale, and synoptic scale.

[32] An interesting feature is that, between 20 and 45 min, the spectral slope is independent of the month (except during the fall). Moreover, the obtained value is close to 5/3, which is the expected value for velocity within a turbulent flow. It could indicate that rain at small scales rain is driven by turbulence. The value is a bit lower than 5/3 possibly because of some zero rain data in time series or because of strong rain cell displacement (two successive points in time at a constant location do not correspond exactly to the same rain cell). This time scale regime (20–45 min) can be related to the minimal time interval encompassing a single and continuous rainfall event. Except for summer months, this scaling range

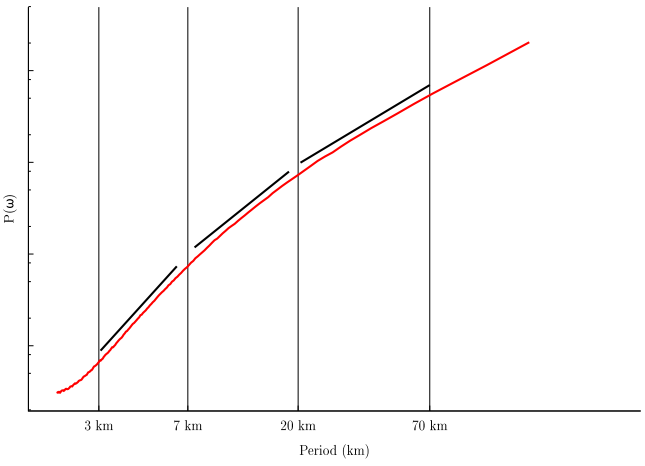

Figure 5. Energy spectral density versus spatial period in a log-log plot.

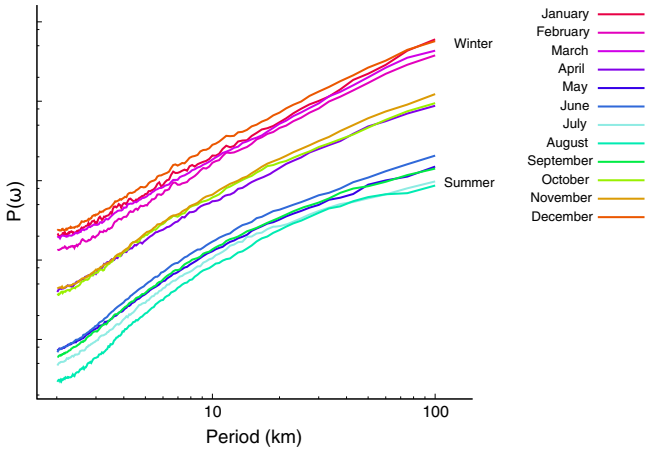

Figure 6. Energy spectral density versus spatial period in a log-log plot by month.

extends until about 3 h despite a slightly lower slope for periods higher than 45 min. An interpretation could be that, during those months, typical duration of rainfall is between a few minutes and 3 h. It is interesting to note that 3 h is the typical duration of mesoscale events (organized convection, front, etc.) as revealed by the analysis of the equations of motion (section 3.2). The slope is slightly lower when periods are higher than 45 min that could be related to the variable duration of rainfall and that, as the period considered becomes longer, more zero rain points are taking into account.

[33] Concerning the summer spectra, we showed that a break appears at 45 min. In section 3.2, we argued that 45 min is the typical time associated to convective scale, and we know that, in summer, most of rain events correspond to convective rain. Thus, lower than 45 min, the scaling range could correspond to a single rainfall events within a convective cell and, between 45 min and 3 h, the scaling range could correspond to the time between consecutive convective cells. Eventually, the break at 3 h could show that, during the summer, mesoscale rain structures also occur.

Table 3. Spatial Spectral Slopes for Winter and Summer Per Scaling Range

Season	3–7 km	7–20 km	20–70 km
Winter	1.55 ± 0.05	1.55 ± 0.05	1.55 ± 0.05
Summer	2.29 ± 0.11	1.55 ± 0.03	0.94 ± 0.07

[34] The break at 1 day appears each month and can be related to the mean time between large scale rain events (for example the time between two fronts on the region). Eventually, the scale range 1–10 days corresponds to the lifetime of synoptical scale structures (i.e., midlatitude cyclone) [*McIlveen*, 1992]. At longer scales than 10 days, the spectral plateau implies that we do not have any correlation between weather precipitating systems, which travel on the region. A possible interpretation is that organized rainfall processes do not exist longer than the synoptical scale processes. This interpretation is supported by the fact that *Lovejoy and Schertzer* [2010] showed, by a semi-empirical approach, that the 10 day scale is the expected value for the transition between synoptical events and spectral plateau in the atmosphere.

[35] During the fall, slope is lower at high frequency. This surprising behavior appears each year taken individually and will be discussed in detail in the next section.

4.2. Spatial Analysis

[36] The spatial extension (the radar coverage) of our data set is much smaller than the temporal one. It is still

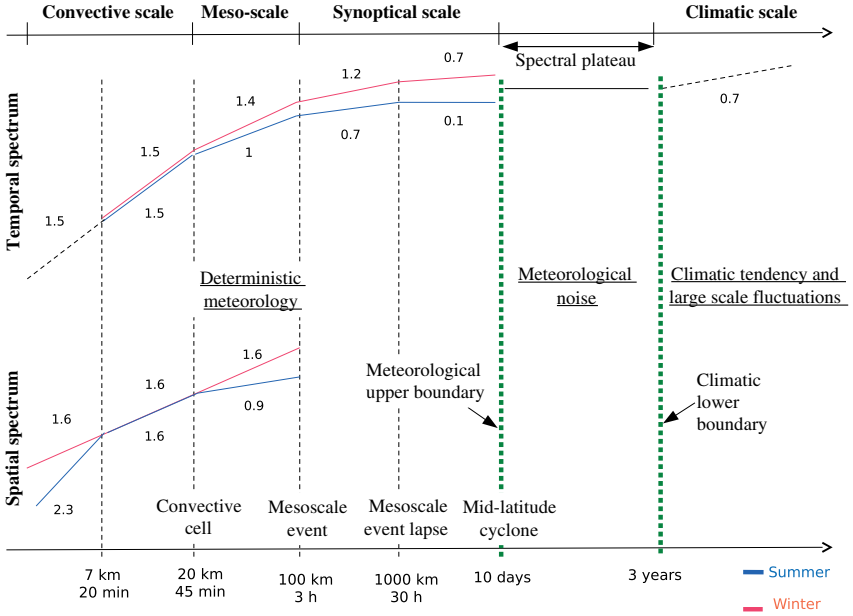

Figure 7. Scheme of spatial and temporal spectra of rainfall with slopes and breaks. We indicated some possible meteorological scales and processes. Dashed lines of the spectra are adapted from *Fraedrich and Larnder* [1993] & *Verrier et al.* [2011]. Note that spatial slopes are estimated by averaging over angles in the 2-D spectra.

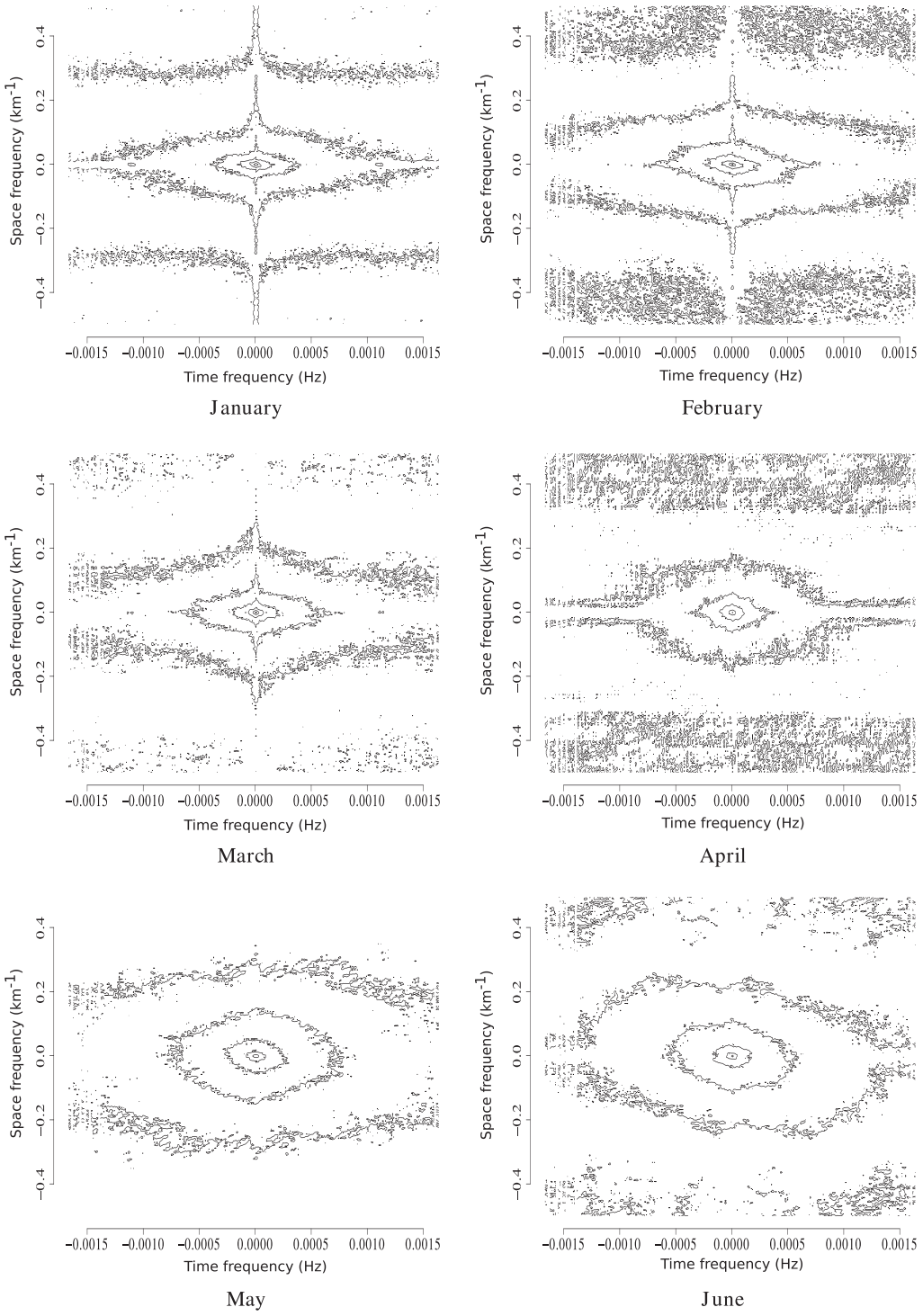

Figure 8. Level map of the logarithm of the power spectral density (x-t) computed between June 2009 and December 2011 (January to June).

possible to study the rainfall scaling behavior for scales lower than the radar area ($40,000$ km^2) and higher than the minimal resolution 1 km^2. As the rainfall field shows a spatial scaling isotropy (see Figure 4), it is equivalent to compute the one-dimensional Fourier spectrum whatever the direction (for any combination of the latitude and longitude). In the present case, for each radar map, two 1D spectra centered on the radar are computed. One along a direction of constant latitude, and one along a direction of constant longitude. Then, the mean of both 1-D spectra for all the radar maps is computed. In the Kolmogorov sense, the power spectrum is defined as the square of the 2-D Fourier spectrum integrated over all angles. It means that for an angle averaged isotropic 2-D spectrum, an extra factor of $2\pi f$ is needed. Nevertheless, this definition can not be interpreted in terms of correlation within the field that makes

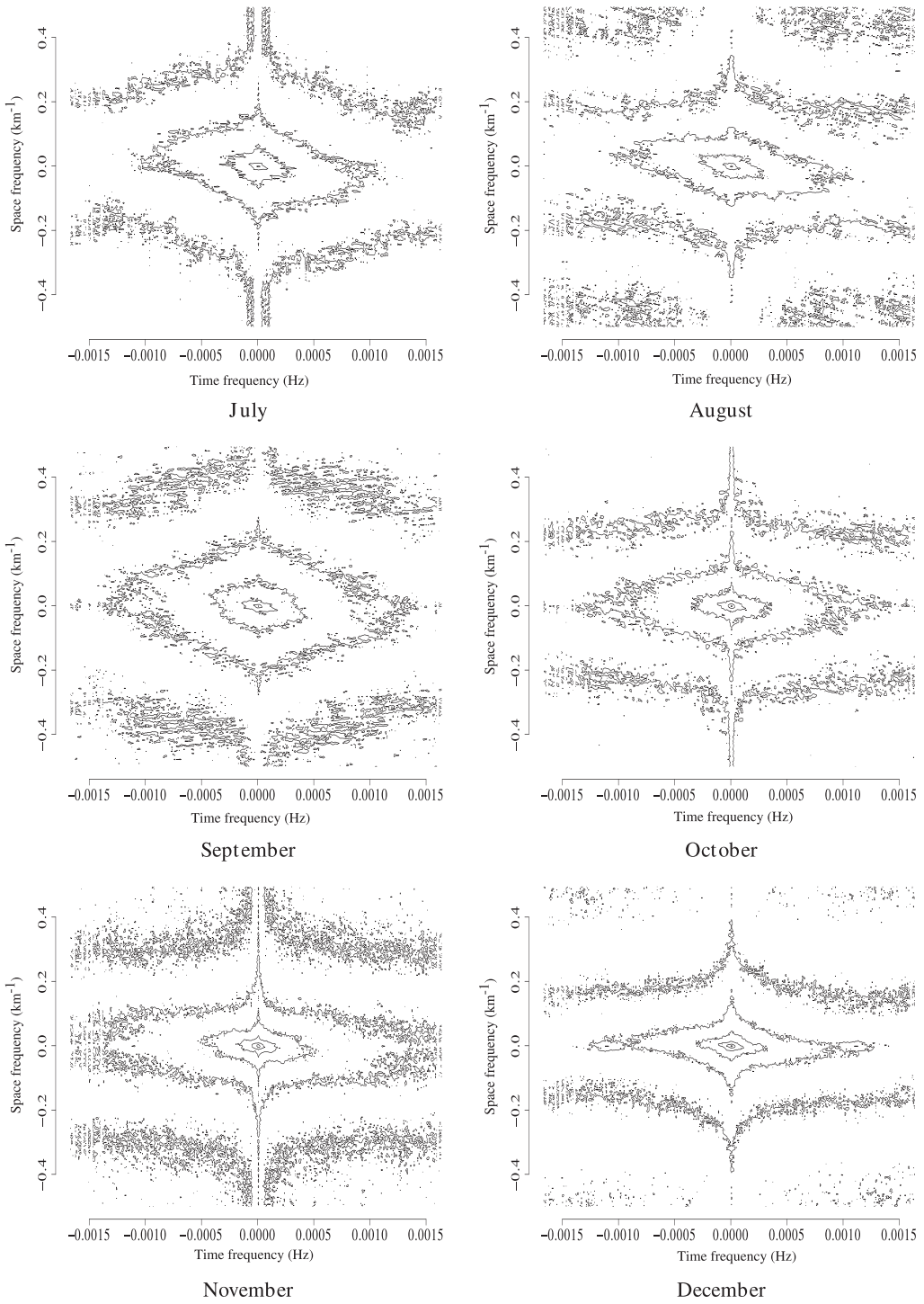

Figure 9. Level map of the logarithm of the power spectral density (x-t) computed between June 2009 and December 2011 (July to December).

difficult an interpretation in terms of meteorological processes. For instance, using this definition, a 2-D spatial noise shows a spectral exponent of –1 without meaning in terms of correlation.

[37] The obtained spatial spectrum is shown in Figure 5. Three scaling regimes are identified between 3 and 70 km. The first one extends from 3 to 7 km with a β exponent of about 2.00. Between 7 and 20 km, the exponent is about 1.50. Between 20 and 70 km, the slope is equal to 1.16. For larger scales, the slope of the spectrum decreases slowly ($\beta \sim 0.92$ between 70 and 200 km) and does not appear to be scaling anymore.

[38] As previously discussed, the equivalent slopes in a Kolmogorov sense are 1, 0.50, and 0.16. These values are lower than the one predicted by Kolmogorov (5/3) and the one computed by *Tessier et al.* [1993], who found a β equal

to 1.45 between 75 m and 10 km for radar reflectivity, and *Verrier et al.* [2010] who reported that the spectrum of African monsoon storms is scaling between 1 and 10 km with a β exponent of 1.47. These authors estimated this exponent on full rain maps. Therefore, the observed slopes are lower probably because of zero rain data effect (radar maps with partial rain coverage).

[39] In Figure 5, we can also see that for scales lower than 3 km, the spectrum becomes flatter. This is related to the minimum scale reachable by the radar resolution (see, for example, the spatial spectrum in *Verrier et al.* [2010]).

[40] As for the temporal analysis, each month is analyzed separately (Figure6). Winter and summer months show very different behaviors. Winter months are scaling from 3 to 70 km with a slope of about 1.55 $\pm$ 0.05, whereas summer months show two breaks at 7 and 20 km (slope: 2.29 $\pm$ 0.11, 1.55 $\pm$ 0.03, and 0.94 $\pm$ 0.07). Other months show a mix signal between winter and summer months. These results are summarized in Table 3.

[41] Spatial scales analyzed correspond to convective scale and mesoscale. As for temporal spectra, the slope of a scaling regime (i.e., 7–20 km) is found to be constant whatever the month. Moreover, for winter months, the slope ($\sim$ 1.55) remains constant between 3 and 70 km. Thus, in winter, a unique scaling regime characterizes the rainfall scaling behavior from 3 to 70 km. This scaling range could be related to the size of a continuous rainfall events (i.e., frontal system), which is wider than 70 km in winter. In summer, the situation is more complex: three scaling regimes are observed (3–7 km, 7–20 km, and 20–70 km). Because 3–7 km scaling regime occurs only in summer, it is probably related to convection. Nevertheless 3–7 km is smaller than the typical size of a convective system in this region ($\sim$20 km), and the slope of this scaling regime is much greater than the slope of the corresponding scaling regime in winter. A possible explanation can be that during convective activity, the main flux is buoyancy variance flux [see *Schertzer and Lovejoy*, 1985] (not the energy flux), which can increase the spectral slope. Another explication could be that turbulence within updraft area is strongly anisotropic. Therefore, the 3 to 7 km scaling regime could be related to the updraft region of the convective cell where atmosphere is strongly anisotropic.

[42] However, the previous interpretations must be handled with care because filtering methods can also affect spectra at small scales. In particular, spatial resolution decreases with distance from the radar. As a result, rain field is smoother when it is far from the radar that can increase spectral slope for small scales.

[43] Another break occurs at 20 km in summer. It probably corresponds to the transition between intra-events and inter-events regimes. Indeed 20 km is the typical size of convective cells in the region. In winter, no break occurs because rainfall is more widespread.

[44] Eventually, the fact that the spectra does not show a clear scaling regime for larger scale than 70 km probably results from radar attenuation.

[45] Most of the authors [e.g., *Menabde et al.*, 1997; *Nykanen and Harris*, 2003; *Nykanen*, 2008] who studied the spatial scaling of the rainfall did not discuss the breaks at 7 and 20 km (*Gires et al.* [2011] mentioned the break at 20 km). It is probably related to the fact that most of the previous studies focused on particular convective storms and not on successive convective precipitating systems including their stratiform zones as we did here.

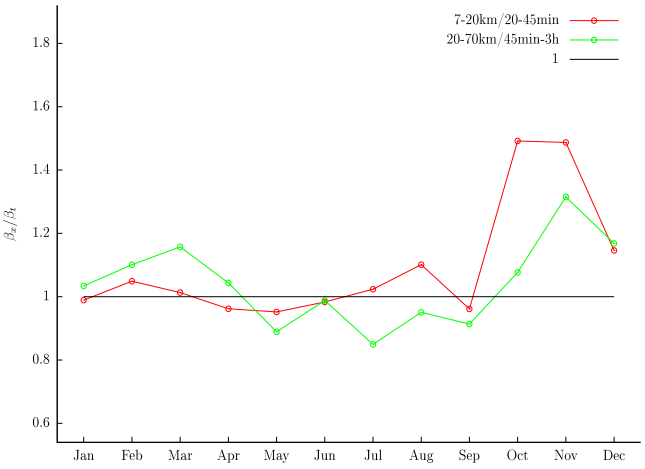

Figure 10. Spectral exponent ratios for each month for scale range 7–20 km/20–45 min and 20–70 km/45 min–3 h.

[46] In the previous section, we showed that temporal spectra have a surprising behavior for small periods during the fall. On the other hand, in this section, we showed that spatial spectra in the fall are very similar to winter spectra. A possible explanation of this behavior follows.

[47] *Rysman et al.* [2012] showed that, in the fall, since the Mediterranean is warmer than land, convection occurs on the Mediterranean and is quickly advected by wind because there is no land barrier. So, a possible explanation could be that cell displacement is too quick relative to sampling time which does not permit to sample a continuous rain cell, and as a result, two successive points in time are not strongly correlated and spectral slope is lower.

[48] As a conclusion, Figure 7 summarizes the main characteristics of the one-dimensional temporal and spatial spectra described in this section. In this figure, we added some part of spectra extracted from other studies at larger and lower scales. In particular, *Fraedrich and Larnder* [1993] showed that for periods greater than 3 years, the spectra rises monotonically. As we showed, for periods greater than 10 days, we do not have any correlation among the data and it could appear surprising to have a correlation at much more larger scales. A possible explanation could be that this correlation is related to the climatic tendency. This tendency could be part of a long-term cycle and be significantly detectable only for time scales greater than 3 years. The spectral plateau between 10 days and 3 years could correspond to an intermediate region where variance between two points does not increase as the temporal lag increases (i.e., successive weather systems do not show any correlation above the region) and where climate tendency is hidden by meteorological noise. As a consequence, we could fix the limit of deterministic meteorology analysis at a period lower than 10 days and the lower boundary of climate analysis at 3 years. It would imply that trying to forecast weather at higher ranges than 10 days based on actual observations might be hopeless. Moreover, we showed that the spectral plateau occurs for periods lower than 10 days in summer. It could explain why forecasts are less accurate in

summer than in winter in the region. Nevertheless, previous interpretations must be handled with care. In particular, we only studied the second-order properties of the rain signal. Additional analysis for other moments are needed in order to check that the decorrelation at 10 days appears for every moment. Moreover, complementary analyses must be conducted on other meteorological parameters and with other methods.

5. Two Dimensional Spectral Analysis

5.1. Space-Time Spectra

[49] As shown previously, one-dimensional analysis is a precious tool to explore the rainfall scaling behavior. However, it does not allow investigations of the relationship between spatial and temporal scales. Few studies used multi-dimension spectral analyses to document rainfall scaling behavior. For instance, *Crane* [1990] evaluated the spatial isotropy of rain for several events. *Tessier et al.* [1993] studied the rain space-time relationship (z-t) using a two-dimensional Fourier transform. *Marsan et al.* [1996] computed x-t and y-t spectra on rainfall data to test their space-time model. *de Michele and Bernardara* [2005] proposed a generalized form of the spectral density function to take into account the space-time anisotropy and to realize a 3-D (x-y-t) fit on four rainfall events.

[50] In the present study, we were interested in the statistical properties that exist between space and time. We used longitude for space component, but latitude could have been identically used because of the spatial scaling isotropy (see Figure 4). We investigated these properties in relation to meteorological processes and their evolution during the year. Note that contrary to previous studies [e.g., *Marsan et al.*, 1996; *Venugopal et al.*, 1999], we do not aim at proposing a model that links space and time.

[51] A two-dimensional fast Fourier transform algorithm is applied on a window of 120 km versus 1 day. As a result, the spectra mainly combine convective scale and mesoscale structures for spatial frequencies and mesoscale and synoptic scale structures for temporal frequencies. The energy spectral density is averaged for every month of the 3 year database.

[52] Figures 8 and 9 present a level map of the logarithm of the obtained power spectral density averaged by month. Note that spectra shown on these maps are not equivalent to 1-D spectra because frequencies are plotted on linear axes. Because of linear axes, most of the periodicities observed on those maps are short (mainly between 2 and 30 km spatially and between 5 min and 2 h temporally). The figures show an elliptical structure and important variability during the year. The pattern evolves during the year from a strong stratification in temporal frequency, for winter months, to an isotropy for summer. As shown in previous sections, in winter, the spatial spectral slope is equal to 1.55 and the temporal slope is equal to 1.5. The spectra appear deformed because of the chosen axis. In summer, the temporal slope is the same but the spatial slope is higher ($\sim$ 1.83). Hence, the spectra look rather isotropic. The main idea here is that computing a 2-D spectrum provides a straightforward way of getting information on rainfall space-time properties and the shape of the 2-D spectra depends on the involved meteorological processes.

[53] These figures reveal another feature: the overall rotation of ellipses. As the Fourier transform results in a $\pi/2$ direct rotation, the ellipse rotation in the frequency space corresponds to a rotation in the real space that is related to the eastward displacement of rain. This can be easily verified using time series of reflectivity map (not shown).

5.2. Space-Time Scaling Anisotropy

[54] The last part of this work is devoted to space-time scaling anisotropy. The knowledge of space-time scaling relationships is of primer interest to understand rainfall internal behavior and evolution.

[55] We computed the spectral exponent ratio for every month for two scaling regimes. The two scaling regimes investigated are 7–20 km versus 20–45 min and 20–70 km versus 45 min–3 h. Figure 10 gives the time evolution of the obtained ratios during the year. The spectral exponent ratio is shown to be equal to 1 (except during the fall). This constancy during the year confirms in an indirect way that the scaling ranges considered in this analysis are part of the same meteorological processes. Moreover, the fact that the ratio equals 1 suggests a similarity in the second-order properties (e.g., correlation) of rainfall.

[56] *Marsan et al.* [1996] and *Pecknold et al.* [2001] showed that the scaling anisotropy coefficient H_t can be derived from spectral slopes β_x and β_t using the following equation:

$$1 - H_t = \frac{\beta_x - 1}{\beta_t - 1} \tag{3}$$

where β_x is computed with integration over angle of 2-D spectrum. H_t is found to be equal to 2 except in the fall. Some other estimations of this coefficient based on different methods gave different values [*Marsan et al.*, 1996; *Deidda*, 2000; *de Montera et al.*, 2010] ($H_t \sim -0.1$, $H_t \sim -0.12$ and $H_t \sim 0.37$). Some downscaling approaches based on scaling space-time cascades assume that when lengths are divided by δ_{xy}, then duration is divided by $\delta_t = \delta_{xy}^{1-H_t}$ and $H_t = 1/3$ is the usual value used [e.g., *Biaou*, 2004; *Gires et al.*, 2012]. The value obtained in this study is larger than these values possibly because of the zero effect and this must be confirmed in future studies.

6. Conclusion

[57] A 3-year rainfall time series of radar maps obtained from an X-band, polarimetric, and Doppler radar was analyzed. The spatial and temporal resolutions are 1 km and 5 min, respectively. These data were analyzed using temporal, spatial, and spatio-temporal power spectral analyses.

[58] One-dimension power spectra in space and time was used to highlight the well-known power law scaling behavior from 5 min to 10 days. Several scaling regimes were found for time and space. Based on meteorological arguments, we interpreted each scaling regimes found with the spectral analysis. In particular, the convective, mesoscale, and synoptic scale regimes impact the temporal spectra whereas the convective and mesoscale regimes impact the spatial spectra. Temporal spectra also showed that the longest period where we found temporal correlation in

rainfall is 10 days. Climatic fluctuations are only detectable for periodicities higher than 3 years. In the second part of the study, we used space-time spectra to investigate the scaling relationship between space and time. We showed that the high variability of 2-D scaling behavior from month to month was due to the various rainfall processes during the year. Moreover, we were able to compute space-time anisotropy coefficient per month and we showed that it is equal to 2.

[59] This analysis provides precious information on spatial and temporal variability of rainfall events in the western Mediterranean region. It suggests that rainfall scaling relationship strongly depends on the encountered weather regime and on the scale. Various weather regimes occur in this region and have clear spectral signatures in space and time. As a result, it seems interesting to check that outputs from weather model are in agreement with each part of the observed rainfall spectrum. Indeed, even if rainfall accumulation seems well-forecasted, one has also to verify that the involved processes are consistent with the simulated field [see *Koh et al.*, 2012; *Gires et al.*, 2012, for examples].

[60] Space-time spectrum appears to be valuable to the investigation of statistical properties and space-time relationships. It can be valuable to statistical downscaling, which is essential to disaggregate spatial and temporal outputs of climate models. In particular, we identified several scaling regimes in time and space. Some downscaling method, such as RainFARM [*Rebora et al.*, 2004], use the spectral information at large scales to infer rain at small scale. They could benefit from the highlighted scaling regimes to be improved. Moreover, we showed that the spectral ratio is equal to 1 except in the fall. This property, if confirmed for other moments and other studies, reveals a straightforward relationship between spatial and temporal scaling behavior of rain, which can be important for numerical model schemes. Indeed, it reveals that relation between scales is identical, in terms of second-order properties, for space and time, which suggests that some parameterizations could be applied identically in space and time (for example, microphysical relations based on a characteristic time could be symmetrically associated to microphysical relations based on characteristic length). It has also implications for the understanding of rainfall spatial and temporal relations over scale. For example, organized convection is a combination of convective cells. All these convective cells have a short lifetime and size, whereas the organized system has a larger lifetime and size. It reveals a relation between space and time properties of rain that depends on the scale and that could be related to the properties identified in this study (spectral ratio equal to 1 for two scaling regimes).

[61] In a future work, larger spatial scales will be considered to study processes at synoptical scales. Moreover, the multiscaling framework will be useful to improve the analysis of this data set. In particular, some parameters of this model, such as codimension, will be helpful in understanding the involved meteorological processes.

[62] **Acknowledgments.** We would like to thank Aymeric Chazottes and Georges Scialom for their insightful comments and for the careful proofreading of this paper. We also thank the three referees for their helpful comments and suggestions, which improved the paper.

References

Atkinson, B. (1981), *Meso-Scale Atmospheric Circulations*, Academic Press, London.

Barros, A. P., G. Kim, E. Williams, and S. W. Nesbitt (2004), Probing orographic controls in the Himalayas during the monsoon using satellite imagery, *Nat. Hazard. Earth Syst. Sci.*, *4*, 29–51.

Berne, A., G. Delrieu, J.-D. Creutin, and C. Obled (2004), Temporal and spatial resolution of rainfall measurements required for urban hydrology, *J. Hydrol.*, *299*, 166–179, doi:10.1016/j.jhydrol.2004.08.002.

Berne, A., G. Delrieu, and B. Boudevillain (2009), Variability of the spatial structure of intense Mediterranean precipitation, *Adv. Water Res.*, *32*, 1031–1042.

Biaou, A. (2004), De la méso-échelle la micro-échelle: Désagrégation spatio-temporelle multifractale des précipitations, Ph.D. thesis, ENSMP.

Boudevillain, B., et al. (2009), Projet Cyprim, Partie I: Cyclogénèse et précipitations intenses en région méditerranéenne: Origines et caractéristiques, *La Météorol.*, *66*, 18–28, doi:10.4267/2042/28828.

Corrsin, S. (1951), On the spectrum of isotropic temperature fluctuations in an isotropic turbulence, *J. Appl. Phys.*, *22*, 469–473, doi:10.1063/1.1699986.

Crane, R. K. (1990), Space-time structure of rain rate fields, *J. Geophys. Res.*, *95*, 2011–2020, doi:10.1029/JD095iD03p02011.

Creutin, J. D., and C. Obled (1982), Objective analyses and mapping techniques for rainfall fields: An objective comparison, *Water Resour. Res.*, *18*, 413–431, doi:10.1029/WR018i002p00413.

de Michele, C., and P. Bernardara (2005), Spectral analysis and modeling of space-time rainfall fields, *Atmos. Res.*, *77*, 124–136, doi:10.1016/j.atmosres.2004.10.031.

de Montera, L., L. Barthès, C. Mallet, and P. Golé (2009), The effect of rain-no rain intermittency on the estimation of the universal multifractals model parameters, *J. Hydrometeorol.*, *10*, 493–506, doi:10.1175/2008JHM1040.1.

de Montera, L., S. Verrier, C. Mallet, and L. Barthès (2010), A passive scalar-like model for rain applicable up to storm scale, *Atmos. Res.*, *98*, 140–147.

Deidda, R. (1999), Multifractal analysis and simulation of rainfall fields in space, *Phys. Chem. Earth B*, *24*, 73–78, doi:10.1016/S1464-1909(98)00014-8.

Deidda, R. (2000), Rainfall downscaling in a space-time multifractal framework, *Water Resour. Res.*, *36*, 1779–1794, doi:10.1029/2000WR900038.

Diss, S., J. Testud, J. Lavabre, P. Ribstein, E. Moreau, and J. Parent du Chatelet (2009), Ability of a dual polarized X-band radar to estimate rainfall, *Adv. Water Res.*, *32*, 975–985.

Fabry, F. (1996), On the determination of scale ranges for precipitation fields, *J. Geophys. Res.*, *101*, 12,819–12,826, doi:10.1029/96JD00718.

Fraedrich, K., and C. Larnder (1993), Scaling regimes of composite rainfall time series, *Tellus A*, *45*(4), 289–298.

Funatsu, B. M., C. Claud, and J.-P. Chaboureau (2009), Comparison between the large-scale environments of moderate and intense precipitating systems in the Mediterranean Region, *Mon. Wea. Rev.*, *137*, 3933–3959, doi:10.1175/2009MWR2922.1.

Gage, K. S., and G. D. Nastrom (1986), Theoretical interpretation of atmospheric wavenumber spectra of wind and temperature observed by commercial aircraft during GASP, *J. Atmos. Sci.*, *43*, 729–740, doi:10.1175/1520-0469(1986)043<0729:TIOAWS>2.0.CO;2.

Gires, A., I. Tchiguirinskaia, D. Schertzer, and S. Lovejoy (2011), Analyses multifractales et spatio-temporelles des précipitations du modèle Méso-NH et des données radar, *Hydrol. Sci. J.*, *56*, 380–396, doi:10.1080/026266672011.564174.

Gires, A., C. Onof, C. Maksimovic, D. Schertzer, I. Tchiguirinskaia, and N. Simoes (2012), Quantifying the impact of small scale unmeasured rainfall variability on urban runoff through multifractal downscaling: A case study, *J. Hydrol.*, *442*, 117–128, doi:10.1016/j.jhydrol.2012.04.005.

Harris, D., M. Menabde, A. Seed, and G. Austin (1996), Multifractal characterization of rain fields with a strong orographic influence, *J. Geophys. Res.*, *101*, 26,405–26,414, doi:10.1029/96JD01656.

Holton, J. (1992), *An Introduction to Dynamic Meteorology*, Academic Press Inc, Waltham.

Hoskins, B. J., and K. I. Hodges (2002), New perspectives on the Northern Hemisphere winter storm tracks, *J. Atmos. Sci.*, *59*, 1041–1061, doi:10.1175/1520-0469(2002)059<1041:NPOTNH>2.0.CO;2.

Kirstetter, P.-E., G. Delrieu, B. Boudevillain, and C. Obled (2010), Toward an error model for radar quantitative precipitation estimation in the Cévennes-Vivarais region, France, *J. Hydrol.*, *394*, 28–41, doi:10.1016/j.jhydrol.2010.01.009.

Koh, T.-Y., B. C. Bhatt, K. K. W. Cheung, C. K. Teo, Y. H. Lee, M. Roth, and Purnawirman (2012), Using the spectral scaling exponent for

validation of quantitative precipitation forecasts, *Meteorol. Atmos. Phys.*, *115*, 35–45, doi:10.1007/s00703-011-0166-4.

Kolmogorov, A. (1941), The local structure of turbulence in incompressible viscous fluid for very large Reynolds' Numbers, *Akad. Nauk SSSR Dokl.*, *30*, 301–305.

Kolmogorov, A. N. (1962), A refinement of previous hypotheses concerning the local structure of turbulence in a viscous incompressible fluid at high Reynolds number, *J. Fluid Mech.*, *13*, 82–85, doi:10.1017/S0022112062000518.

Le Bouar, E., E. Moreau, and J. Testud (2008), The rain accumulation product from the X-band polarimetric radar HYDRIX, WRaH (Weather Radar and Hydrology).

Lebel, T., G. Bastin, C. Obled, and J. D. Creutin (1987), On the accuracy of areal rainfall estimation: A case study, *Water Resour. Res.*, *23*, 2123–2134, doi:10.1029/WR023i011p02123.

Lovejoy, S., and D. Schertzer (2008), Turbulence, raindrops and the $l^{1/2}$ number density law, *New J. Phys.*, *10*(7), 075017, doi:10.1088/1367-2630/10/7/075017.

Lovejoy, S., and D. Schertzer (2010), Towards a new synthesis for atmospheric dynamics: Space-time cascades, *Atmos. Res.*, *96*, 1–52.

Mandapaka, P. V., P. Lewandowski, W. E. Eichinger, and W. F. Krajewski (2009), Multiscaling analysis of high resolution space-time lidar-rainfall, *Nonlinear Processes Geophys.*, *16*, 579–586.

Mandapaka, P. V., U. Germann, and L. Panziera (2012), Diurnal cycle of precipitation over complex Alpine orography: Inferences from high-resolution radar observations, *Q. J. R. Meteorolog. Soc.*, *139*, 1025–1046, doi:10.1002/qj.2013.

Marsan, D., D. Schertzer, and S. Lovejoy (1996), Causal space-time multifractal processes: Predictability and forecasting of rain fields, *J. Geophys. Res.*, *101*, 26,333–26,346, doi:10.1029/96JD01840.

McIlveen, R. (1992), *Fundamentals of Weather and Climate*, Chapman & Hall, London, UK.

Menabde, M., A. Seed, D. Harris, and G. Austin (1997), Self-similar random fields and rainfall simulation, *J. Geophys. Res.*, *102*, 13,509–13,516, doi:10.1029/97JD00915.

Molinié, G., D. Ceresetti, S. Anquetin, J. D. Creutin, and B. Boudevillain (2012), Rainfall regime of a mountainous Mediterranean Region: Statistical analysis at short time steps, *J. Appl. Meteorol. Climatol.*, *51*, 429–448, doi:10.1175/2011JAMC2691.1.

Moreau, E., J. Testud, and E. Le Bouar (2009), Rainfall spatial variability observed by X-band weather radar and its implication for the accuracy of rainfall estimates, *Adv. Water Res.*, *32*, 1011–1019.

Moreau, K., and A. Roumagnac (2010), Feedback on floods in Var, south of France, 15th June 2010: Different societal impacts and responses linked to levels of prevention, organization and information, *12th Plinius Conference on Mediterranean Storms, held September 1-4, 2010 in Corfu Island, Greece*, http://meetings.copernicus.org/plinius12, id.Plinius12-24.

Nykanen, D. K. (2008), Linkages between orographic forcing and the scaling properties of convective rainfall in Mountainous Regions, *J. Hydrometeorol.*, *9*, 327–347, doi:10.1175/2007JHM839.1.

Nykanen, D. K., and D. Harris (2003), Orographic influences on the multiscale statistical properties of precipitation, *J. Geophys. Res.*, *108*(D8), 8381, doi:10.1029/2001JD001518.

Obukhov, A. (1949), Structure of the temperature field in a turbulent flow, *Izv. Akad. Nauk S.S.S.R., Ser Geograf. Geofiz.*, *13*, 58–69.

Olsson, J. (1995), Limits and characteristics of the multifractal behaviour of a high-resolution rainfall time series, *Nonlinear Processes Geophys.*, *2*, 23–29.

Olsson, J. (1998), Evaluation of a scaling cascade model for temporal rainfall disaggregation, *Hydrol. Earth Syst. Sci.*, *2*, 19–30.

Olsson, J., J. Niemczynowicz, and R. Berndtsson (1993), Fractal analysis of high-resolution rainfall time series, *J. Geophys. Res.*, *98*, 23,265–23,274, doi:10.1029/93JD02658.

Olsson, J., V. P. Singh, and K. Jinno (1999), Effect of spatial averaging on temporal statistical and scaling properties of rainfall, *J. Geophys. Res.*, *104*, 19,117–19,126, doi:10.1029/1999JD900271.

Orlanski, I. (1975), A rational subdivision of scales for atmospheric processes, *Bull. Am. Meteorol. Soc.*, *56*(5), 527–530.

Over, T. M., and V. K. Gupta (1994), Statistical analysis of mesoscale rainfall: Dependence of a random cascade generator on large-scale forcing, *J. Appl. Meteorol.*, *33*, 1526–1542, doi:10.1175/1520-0450(1994)033<1526:SAOMRD>2.0.CO;2.

Over, T. M., and V. K. Gupta (1996), A space-time theory of mesoscale rainfall using random cascades, *J. Geophys. Res.*, *101*, 26,319–26,332, doi:10.1029/96JD02033.

Pecknold, S., S. Lovejoy, and D. Schertzer (2001), Stratified multifractal magnetization and surface geomagnetic fields, II. Multifractal analysis and simulations, *Geophys. J. Int.*, *145*, 127–144, doi:10.1111/j.1365-246X.2001.00345.x.

Perica, S., and E. Foufoula-Georgiou (1996), Linkage of scaling and thermodynamic parameters of rainfall: Results from midlatitude mesoscale convective systems, *J. Geophys. Res.*, *101*, 7431–7448, doi:10.1029/95JD02372.

Pettersen, S. (1956), *Weather Analysis and Forecasting*, vol. 1, McGraw-Hill Company, New York and London.

Purdy, J. C., D. Harris, G. L. Austin, A. W. Seed, and W. Gray (2001), A case study of orographic rainfall processes incorporating multiscaling characterization techniques, *J. Geophys. Res.*, *106*, 7837–7846, doi:10.1029/2000JD900622.

Rebora, N., L. Ferraris, J. von Hardenberg, and A. Provenzale (2004), Rainfall downscaling by a phase-conserving, nonlinearly-transformed autoregressive model: Validation on radar precipitation estimates, *AGU Spring Meeting Abstracts*, p. A2.

Rebora, N., L. Ferraris, J. von Hardenberg, and A. Provenzale (2006), Rainfall downscaling and flood forecasting: A case study in the Mediterranean area, *Nat. Hazard. Earth Syst. Sci.*, *6*, 611–619.

Rysman, J.-F., E. Moreau, and Y. Lemaître (2012), X-band polarimetric and Doppler radar observations of heavy precipitation events over the Mediterranean region (France), *ERAD 2012,* Toulouse, France.

Schertzer, D., and S. Lovejoy (1985), *The Dimension and Intermittency of Atmospheric Dynamics*, 7-33 pp., B. Launder, New York.

Schmitt, F., and C. Scholz (1995), Scaling invariance of crack surfaces, *J. Geophys. Res.*, *100*, 5953–5973, doi:10.1029/94JB02885.

Tessier, Y., S. Lovejoy, and D. Schertzer (1993), Universal multifractals: Theory and observations for rain and clouds, *J. Appl. Meteorol.*, *32*, 223–250, doi:10.1175/1520-0450(1993)032<0223:UMTAOF>2.0.CO;2.

Testud, J., E. Le Bouar, E. Obligis, and M. Ali-Mehenni (2000), The rain profiling algorithm applied to polarimetric weather radar, *J. Atmos. Oceanic Technol.*, *17*(3), 332–356.

Testud, J., J. Lavabre, S. Diss, P. Tabary, and G. Scialom (2007), 2007: HYDRIX radar in FRAMEA—Evaluation of an X-band polarimetric radar using a quasi-colocated S band radar and a rain gauge network, paper presented at International Symposium on X-Band Weather Radar Network, Natl. Res. Inst. for Earth Sci. and Disaster Prev., Tsukuba, Japan.

Venugopal, V., E. Foufoula-Georgiou, and V. Sapozhnikov (1999), A space-time downscaling model for rainfall, *J. Geophys. Res.*, *104*, 19,705–19,722, doi:10.1029/1999JD900338.

Verrier, S., L. de Montera, L. Barthès, and C. Mallet (2010), Multifractal analysis of African monsoon rain fields, taking into account the zero rain-rate problem, *J. Hydrol.*, *389*, 111–120, doi:10.1016/j.jhydrol.2010.05.035.

Verrier, S., C. Mallet, and L. Barthès (2011), Multiscaling properties of rain in the time domain, taking into account rain support biases, *J. Geophys. Res.*, *116*, D20119, doi:10.1029/2011JD015719.

Wernli, H., and C. Schwierz (2006), Surface cyclones in the ERA-40 dataset (1958–2001). Part I: Novel identification method and global climatology, *J. Atmos. Sci.*, *63*, 2486–2507, doi:10.1175/JAS3766.1.